Bhargav Karamched

Research Statement

Synopsis

I am an applied mathematician and a biophysicist. My main interests lie in elucidating ***fundamental principles*** underlying a variety of biological processes using mathematical models. My current work is in two fields: synthetic biology and decision making. My work in synthetic biology consists of describing collective behavior in populations of microbial consortia dynamically evolving in microfluidic devices. From a biological perspective, this involves many different levels of description from the biochemical reactions that control gene network activation states at the single cell level to communication between bacterial cells through quorum sensing molecules. On the decision-making side, I seek to generalize the classical drift-diffusion framework for evidence accumulation by an optimal observer to include a network of optimal observers making independent observations and exchanging social information. Hence, we seek to understand the circumstances where collective decision-making benefits the members of a group and where it is detrimental. Previously, for my doctoral work, I worked on problems involving the transport and delivery of materials to localized areas within cells and understanding the consequences of breakdown in these transport processes. From a modeling perspective, my work draws upon a wide range of techniques from applied mathematics and theoretical physics including differential equations, dynamical systems theory, stochastic processes, numerical analysis, Bayesian inference, and non-equilibrium statistical physics.

Cell Alignment in Extended Microfluidic Traps

A central goal of synthetic biology is the construction of practical, engineered genetic circuits for medical and industrial applications. Critical to this goal is the elucidation of the fundamental mechanisms that govern gene regulation at all levels. Populations of *E. coli* cells trapped in microfluidic devices can be used to study genetic signaling networks and understand how information is communicated between genetic modules distributed across two or more strains of bacteria. In extended microfluidic traps, populations are not well-mixed; therefore, spatiotemporal patterning of distinct bacterial strains plays an important role in inter-strain communication. For example, multi-strain consortia of *E. coli* in open, rectangular microfluidic traps form single-strain bands orthogonal to the long side of the trap (Fig. 1) [1]. The distribution of such bands can affect the efficiency of communication between distinct strains of bacteria due to the limited diffusivity of quorum sensing molecules. Understanding the mechanisms underlying this emergent order is therefore important for engineering synthetic gene circuits with desired properties.

We developed an analytically tractable spatial Moran model (SMM) that captures essential features of the dynamics of growing populations of *E. coli* cells and provides insight into the emergence of these single-strain bands [2]. These capsule-shaped bacterial cells tend to grow more slowly in crowded environments; that is, cells in the center of a trap grow slower than cells along the boundary [4]. We model the microfluidic trap as an $M \times N$ lattice and the cells as oriented particles on the lattice. The cells are in one of two orientations: horizontal or vertical. These cells grow along the major axis of their bodies asymmetrically. We assume a cell's growth rate in a given direction is a monotonically decreasing function of the distance the cell is from the boundary in that direction. The SMM shows that provided this growth-rate dampening due to crowding is sufficiently strong, cells align orthogonally to the long side of the trap, as seen in experiments. However, if the dampening is sufficiently small, a phase transition occurs and cells align *parallel* to the long side of the trap.

The time evolution of the microscopic configurations of the lattice are described by a master equation. Specifically, we characterize the time evolution of the lattice by tracking occupation numbers for each lattice site. Denote by $n_{ij} \in \{0, 1\}$ the state of the ij-th site at time t, so that $n_{ij} = 1$ ($n_{ij} = 0$) corresponds to a site occupied by a vertical (horizontal) cell. The probabilities $p_{ij}(t) = P(n_{ij} = 1 \text{ at time } t)$ evolve according to the master equation

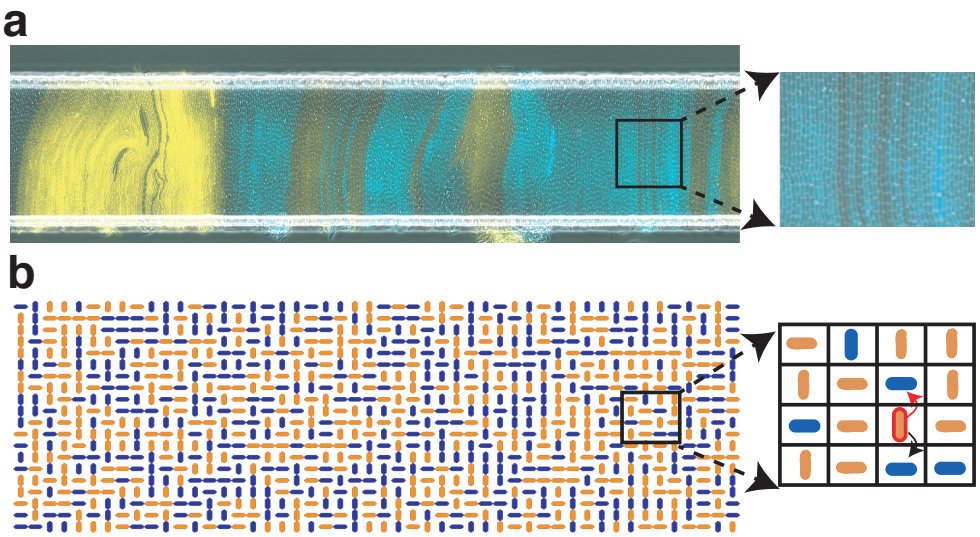

Figure 1: *(a) A monolayer of* E. Coli *in an open microfluidic trap with cells aligned orthogonally to the trap's long side. Colors represent distinct strains. (b) In our spatial Moran model cell growth is directional and location dependent: The outlined vertical cell can grow only upward or downward at a location-dependent rate. The red arrow indicates growth direction, so the cell above will be replaced by a descendant of the outlined cell. We model single strain populations, but use the same color for mother and daughter cells for visualization.*

$$\begin{aligned}\frac{dp_{ij}}{dt} &= v_\kappa^+(i-1)p(n_{(i-1)j}=1,n_{ij}=0,t) + v_\kappa^-(i+1)p(n_{(i+1)j}=1,n_{ij}=0,t)\\ &\quad - h_\kappa^+(j-1)p(n_{i(j-1)}=0,n_{ij}=1,t) - h_\kappa^-(j+1)p(n_{i(j+1)}=0,n_{ij}=1,t),\end{aligned} \tag{1}$$

where $p(n_{ij}, n_{kl}, t)$ are joint occupation probabilities at time t. The first two terms in Eq. 1 correspond to horizontal-to-vertical cell transitions through displacement by a descendant from a cell either above or below. The second two terms describe the opposite transition. The rates $v_\kappa^\pm(i)$ represent a vertical cell's propensity to grow toward the top or the bottom of the trap when it is located in the ith row. The rates $h_\kappa^\pm(j)$ are defined similarly for horizontal cells in the lattice. Growth rates are determined by a one-parameter family of functions, with the parameter $\kappa \in [0,\infty)$ characterizing the population's impact on growth. This family can be general, but we assume that growth rates are positive and satisfy three conditions: (1) There exists a $\lambda \in (0,\infty)$ such that $v_\kappa^\pm(i), h_\kappa^\pm(j) \to \lambda$ as $\kappa \to 0$ for all i, j; (2) Maximal growth rates occur at the boundaries, $v_\kappa^+(M) = v_\kappa^-(1) = h_\kappa^+(N) = h_\kappa^-(1) = \lambda$; (3) $v_\kappa^\pm(i)$, $h_\kappa^\pm(j)$ decrease monotonically with distance from the boundary that maximizes their value. Condition (1) states that cells grow uniformly at rate λ in the absence of interactions ($\kappa = 0$). Conditions (2) and (3) reflect a cell's tendency to grow toward the nearest boundary and growth rate dampening from cells obstructing growth in a certain direction. Stochastic simulations of the SMM are in agreement with solutions to Eq. 1 in the different parameter regimes. In particular, both suggest that there exists a critical κ^* value wherein a transition between alignment orthogonally to the long boundary and parallel to the long boundary occurs.

To calculate κ^* explicitly, we average Eq. 1 over all lattice sites to obtain a mean field model. Averaging the master equation over all i, j shows that n, the fraction of vertical cells, obeys a logistic equation,

$$\frac{dn}{dt} = \underbrace{2\Big(\bar{v}_\kappa\big(1-\frac{1}{M}\big) - \bar{h}_\kappa\big(1-\frac{1}{N}\big)\Big)}_{\mu(\kappa,M,N)} n(1-n), \tag{2}$$

and $n(t) = \exp(\mu(\kappa,M,N)t)/(1+\exp(\mu(\kappa,M,N)t)$. $\bar{v}_\kappa, \bar{h}_\kappa$ are the average growth rates in the vertical, and horizontal directions, respectively. This agrees with the averaged solutions to Eq. 1 and SMM simulations averaged over realizations (see Fig. 2).

From Eq. 2 it is clear that the all-vertical and all-horizontal equilibria exchange stability when $M = N$. However, Eq. 2 provides insight into the underlying mechanism of spatial order. In particular, the growth rate, $\mu(\kappa, M, N)$, manifests as a competition between cell-cell interactions in the average growth rates and boundary

effects. Therefore, there exists a critical κ^* value at which boundary effects dominate cell-cell interactions. For fixed M, N, this transition point satisfies $\mu(\kappa^*, M, N) = 0$.

We show how κ^* scales with trap size for different interaction kernels. To reduce parameter number, we fix M and N and use a single parameter, s, to determine lattice dimensions as $sM \times sN$. We find that for exponential interaction kernels of the form $v_\kappa^+(i) = \lambda e^{-\kappa(M-i)}$,

$$\kappa^* \sim 2/(MNs^2) \sim s^{-2}. \tag{3}$$

For interaction kernels of the form $v_\kappa^+(i) = \lambda/(1+\kappa(M-i)^\alpha), \alpha \in (0,\infty)$,

$$\kappa^* = \frac{(\alpha+1)(N-M)}{s^{\alpha+1}MN(N^\alpha - M^\alpha)} \sim s^{-(\alpha+1)}$$

for large s.

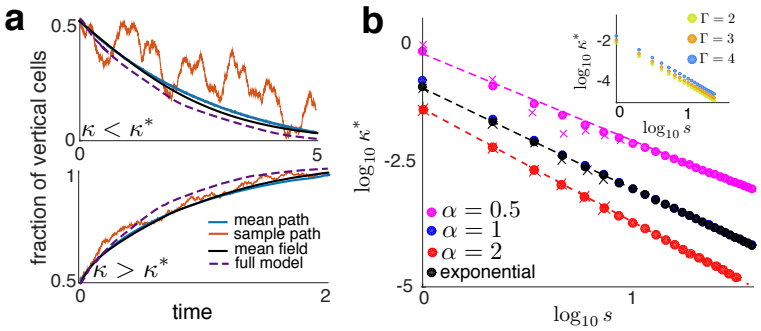

Figure 2: *(a) Comparison of MF solutions with averages over realizations of the SMM ($N = 20$, $M = 10$) . (b) κ^* as a function of s for different interaction kernels. Dots represent κ^* values from Eq.* (2)*. X's were obtained numerically from simulations of the SMM using bisection. Dashed line were obtained using Eq.* (3)*. Inset: κ^* as a function of s for different aspect ratios, $\Gamma \equiv M/N$.*

From a mathematical perspective, the SMM is of interest because it is completely solvable under a reasonable mean-field approximation. That is, critical parameter values can be calculated explicitly as a function of system size. Models that show emergence of patterns yet are completely solvable are rare. Furthermore, the model formulation is general and can be useful in analyzing the dynamics of anisotropically growing multi-species systems in confined environments.

Main result: Our SMM shows that equilibrium alignment of cells is a tug-of-war between boundary effects and growth-rate dampening: boundary effects pull cell alignment to be opposite of what is observed experimentally. Hence, our model suggests that the driving force for orthogonal alignment of cells is growth-rate modulation at the cellular level. Importantly, my work suggests that crowding-induced growth-rate modulation *must* occur at the individual cell level so that orthogonal bands of cells form at the population level, as observed in the experiments. Furthermore, my work suggests that cell interactions in such a trap are *strong*. Bringing this idea to light will be important for experimentalists because the consideration of cell interactions is an important factor in designing experiments.

Future Work

Our model is simple enough to modify to describe a variety of situations. Strains communicate via quorum sensing molecules. We hope to couple our model of *E. coli* cells in extended microfluidic traps with equations describing the dynamics of quorum sensing molecules and how it impacts communication between cells of distinct strains. For example, we can incorporate quorum sensing dynamics in the master equation formulation. Let $q_k(i,j)$ denote the concentration of a quorum sensing molecule at site ij that has been produced by a cell belonging to the strain k. The dynamics can be described by

$$\frac{dq_k(i,j)}{dt} = \lambda p_{ij}^k - \gamma q_k(i,j) + D(q(i+1,j) + q(i-1,j) + q(i,j+1) + q(i,j-1) - 4q(i,j)), \tag{4}$$

Experimentally, the set up for more than two strains of bacteria is very challenging. Our model is therefore ideal to predict what may happen when a large number of distinct strain populations interact in extended microfluidic traps.

At the experimental level, we hope to ***control*** the emergence of spatiotemporal patterns in extended microfluidic devices. The means of achieving such control will be elucidated by our model coupled with agent-based models and continuum models. For example, we have predicted that by allowing distinct strains of bacteria to have distinct cellular aspect ratios, we can control which strain in the microfluidic trap achieves a higher fitness level, thereby driving the other to extinction.

Finally, since the SMM's formulation is quite general, its applicability to a variety of situations is apparent. For example, we can also examine spatiotemporal dynamics of cancer tumor development and how to treat such tumors with virotherapy.

Decision-Making in Networks

A fundamental question in neuroscience is how organisms use sensory and social information to make decisions. Yet few mathematical models of decision making account for both types of information. Popular evidence accumulation models describe an ideal observer using a sequence of sensory measurements to choose among alternatives [5]. However, these models describe an observer in isolation, whereas decisions are often made in groups. For example, animals observe one another when they forage. Stock traders, while not privy to all of their competitor's information, can still observe each other's decisions. It is thus natural to ask how an observer should combine private measurements with social information to make decisions.

We developed a normative model for collective decision making on a network of agents performing a two-alternative forced choice (2AFC) task [3]. We assume that each agent accumulates evidence privately until it makes a choice (Fig. 3). This choice is observed by all of its neighbors on the network. Thus, information flow is described by a directed network, and each deciding agent communicates its decision to those observing it. In this simplified setup, the computations of rational agents can be intuitively explained, but can become extremely complex. For example, when decision thresholds are not symmetric, even *non-decision* on an agent's part provides evidence in favor of one of the two choices to the remaining agents. In recurrent networks, exchange of social information manifests as an equilibration process until all agents understand where each agent's proclivity for a given decision lies–a common knowledge situation. Our model bridges abstractions used in the economics literature and the evidence accumulator models used widely in neuroscience.

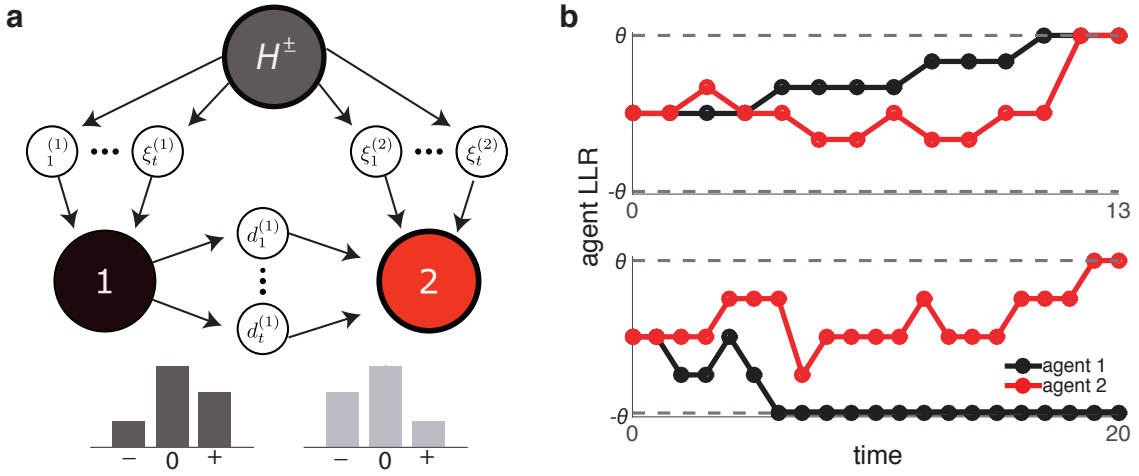

Figure 3: *A pair of unidirectionally coupled agents deciding between the states H^+ and H^- on the basis of private and social evidence. (a) Schematic of the information flow in the network. Agent 1 accumulates its own observations which result in a sequence of decision states that is observed by agent 2. In addition, agent 2 gathers its own observations to make a decision. (b) Sample trajectories for the log likelihood ratios (LLRs) of the agents. Decisions are made when an agent's belief (LLR) crosses a threshold, $\theta_{\pm} = \pm\theta$ in this case. Agent 1's expression of its decision is reflected in an abrupt jump in agent 2's belief.*

Main Result: Our model predicts that including social information in one's evidence for making a decision increases the accuracy of one's decisions and lowers the decision time required to make that decision. These

benefits are more pronounced when observations are very noisy. When observations are reliable, social information is less beneficial.

Future Work

We have a general framework for describing social information flow through a network of N agents. We seek to use this model to describe situations where social information is beneficial or detrimental. For example, ideal observers arranged in a particular network topology may undergo herding behavior wherein a decisive individual choosing a suboptimal decision causes all other members of the network to agree with them, thereby cause collective suboptimal behavior. On the other hand, a decisive individual's decision may be overturned by social information if other members of the network understand that no one agrees with the initial decider.

The stochastic models developed in [3] are all discrete. It is of mathematical interest develop a continuum model of collective optimal decision making. Such models are particularly useful when analyzing decision-making in all-to-all networks, or cliques. Consider a clique of N agents. The ith agent's evidence y^i, $1 \leq i \leq N$ evolves according to the Langevin equation

$$dy^i = gdt + \sigma dW_i \tag{5}$$

where g is a drift component stemming from the Kullback-Leibler divergence between the measurement distributions of the environment conditioned on the true state of the environment $H^{\pm}$ and W_i is a Wiener process. The stochastic processes are independent until the first decision is made. It turns out that the expected time for the first decision amongst N agents evolving according to Eq. 5, τ_N, scales with N as

$$\tau_N = \frac{\theta^2}{4 \ln N}, \tag{6}$$

where θ represents a threshold value corresponding to the amount of evidence required for an agent to make a decision. Hence Eq. 5 is defined on the interval $(-\theta, \theta)$ with absorbing boundaries. $y^i \geq \theta$ means agent i has selected H^+ as its decision, and $y^i \leq -\theta$ means agent i has selected H^- as its decision.

Once the first decision is made, all remaining agents receive a kick to their evidence equal to $\pm\theta$, depending on which decision the first decider made. Such a decision will trigger a wave of deciders that agree with the initial decider. The remaining undecided agents after the first kick now have more information in their decision making. They know how many agents agreed with the first decider and how many are cynical still. If the number of agents undecided after the kick of evidence is greater than the number of agents agreeing with the first decider, the remaining agents will choose the opposite choice. A natural question therefore is to ask what fraction of the clique chooses correctly as $N \to \infty$.

Reliability Failure in Glucose-Insulin Systems

At a fundamental level, the goal of biomedicine is about robust, stable prediction. For instance, pharmaceutical interventions are introduced when they are ***predicted*** to, at best, help, and at worst, do no harm to a patient. Robust, stable, ***reliable*** prediction rests on the following assumption: given a set of initial conditions and parameters, the response to an input will be the same and that some amount of noisiness in the input, initial conditions, or parameters will not significantly affect the statistical properties of the response. These assumptions are fundamental to how biomedicine works. For example, the exact timing of a treatment—up to seconds—or the exact size of the intervention—100 versus 100.1 mg of a drug—will not wildly change the outcome or the treatment.

Rank-one-based shear-induced chaos or uncertainty (SIU) [6] challenges this fundamental assumption because it destroys predictability of the response of a system to a given input subject to minimal noise. SIU, or the sensitivity of an invariant density to perturbations of an orbit along the orbit, occur under at least two conceptual scenarios: ***(i)*** when there is an invariant set that corresponds to a periodic orbit and a related Hopf bifurcation, and ***(ii)*** near a fixed point with invariant-like sets that resemble invariant sets corresponding to a periodic orbit (Fig. 4). The practical implication of SIU is the exact timing of the intervention, or the exact size

of the intervention, can significantly alter the statistical properties of the response, making the system difficult to ***predict***, ***understand*** or ***interpret***.

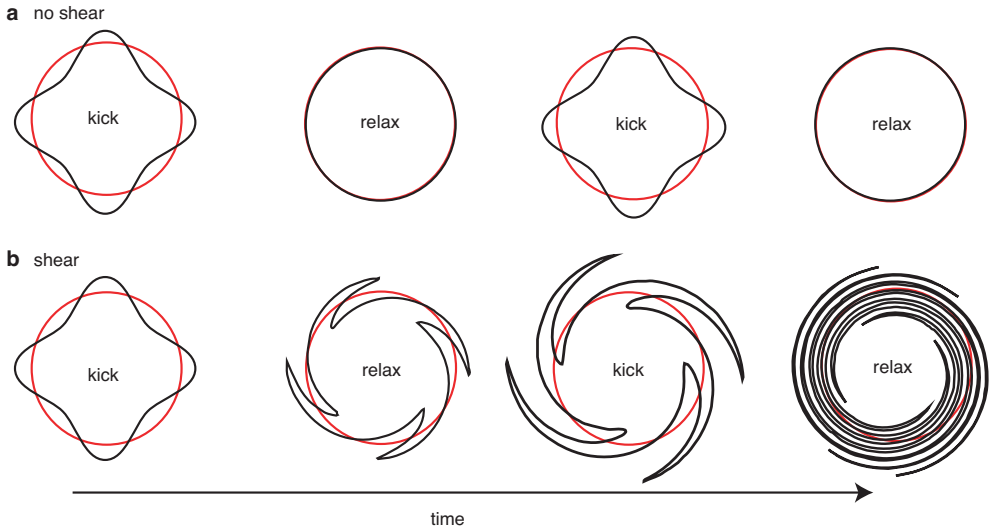

Figure 4: *Schematic of SIU. In the absence of shear, perturbing a system away from a limit cycle causes relaxation back to a limit cycle that is diffeomorphic to the original. In the presence of shear, perturbing a limit cycle will cause it to bend, twist, and stretch. As more and more perturbations are introduced to the system, the attracting set becomes a* ***strange attractor****.*

Many physiologically and clinically important systems are oscillatory, meaning they correspond to noisy periodic orbits, have damping, and are driven. For example, the glucose-insulin system, a subsystem of the the endocrine system, has continuous periodic orbits under continuous nutrition infusion, fixed points, at least one Hopf-like bifurcation allowing for the potential to estimate shear, damping from nutrition utilization, driving from nutrition input, and perturbations off of periodic orbits from meal ingestion. These are all features present in standard rank-one, SIU analysis. Additionally, as is the case for many important physiological systems, the glucose-insulin system has delay variables, a property that is not well understood in the context of rank-one theory. It is within this context that we can explore the potential impact that SIU can have on prediction and understanding in both a clinical and a physiological setting.

A standard model of glucose-insulin dynamics is the Ultradian model [7]. The primary state variables are the glucose concentration G, the plasma insulin concentration I_p, and the interstitial insulin concentration I_i; these three state variables are appended with a three stage filter (h_1, h_2, h_3) which reflects the response of the plasma insulin to glucose levels. The resulting ordinary differential equations take the form:

$$\frac{dI_p}{dt} = f_1(G) - E\left(\frac{I_p}{V_p} - \frac{I_i}{V_i}\right) - \frac{I_p}{t_p} \tag{7a}$$

$$\frac{dI_i}{dt} = E\left(\frac{I_p}{V_p} - \frac{I_i}{V_i}\right) - \frac{I_i}{t_i} \tag{7b}$$

$$\frac{dG}{dt} = f_4(h_3) + I_G(t) - f_2(G) - f_3(I_i)G \tag{7c}$$

$$\frac{dh_1}{dt} = \frac{1}{t_d}\left(I_p - h_1\right) \tag{7d}$$

$$\frac{dh_2}{dt} = \frac{1}{t_d}\left(h_1 - h_2\right) \tag{7e}$$

$$\frac{dh_3}{dt} = \frac{1}{t_d}\left(h_2 - h_3\right) \tag{7f}$$

The ***major*** parameters include: ***(i)*** E, a rate constant for exchange of insulin between the plasma and remote compartments; ***(ii)*** I_G, the exogenous (externally driven) glucose delivery rate; ***(iii)*** t_p, the time constant for plasma insulin degradation; ***(iv)*** t_i, the time constant for the remote insulin degradation; ***(v)*** t_d, the delay time between plasma insulin and glucose production; ***(vi)*** V_p, the volume of insulin distribution in the plasma; ***(vii)***

V_i, the volume of the remote insulin compartment; ***(viii)*** V_g, the volume of the glucose space. $f_1(G)$ represents the rate of insulin production; $f_2(G)$ represents insulin-independent glucose utilization; $f_3(I_i)G$ represents insulin-dependent glucose utilization; $f_4(h_3)$ represents delayed insulin-dependent glucose utilization;

$$f_1(G) = \frac{R_m}{1 + \exp(\frac{-G}{V_g c_1} + a_1)} \tag{8}$$

$$f_2(G) = U_b(1 - \exp(\frac{-G}{C_2 V_g})) \tag{9}$$

$$f_3(I_i) = \frac{1}{C_3 V_g}(U_0 + \frac{U_m - U_0}{1 + (\kappa I_i)^{-\beta}}) \tag{10}$$

$$f_4(h_3) = \frac{R_g}{1 + \exp(\alpha(\frac{h_3}{C_5 V_p} - 1))} \tag{11}$$

$$\kappa = \frac{1}{C_4}(\frac{1}{V_i} - \frac{1}{E t_i}) \tag{12}$$

The nutritional driver of the model $I_G(t)$ is continuously fed to the system.

$$I_G(t) = I_0 + \sum_{n \in \mathbb{N}} A_n \delta(t - T_n), \tag{13}$$

where I_0 is a basal nutritional input for the system, T_n is the time of the nth feeding, and A_n is the amount of carbohydrate in that meal. In Fig. 5 we perform simulations where we fix $A_n = A$ and $T_n = T$ and investigate dynamical behavior of the Ultradian model. We find behavior that is consistent with SIU in this model, which suggests that maintaining stable glucose levels for diabetic patients may be more challenging than it seems, as glucose oscillations grow chaotic if time between meals grows.

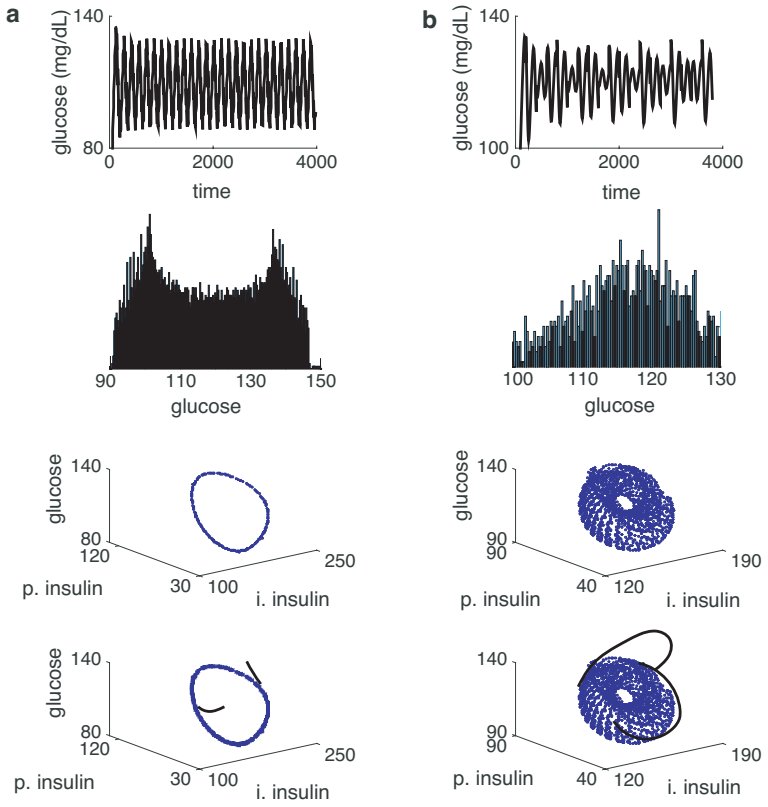

Figure 5: *Time series (top row), glucose invariant densities (second row) and projection of phase space (third and bottom rows) for the kicked Ultradian oscillating system. Also plotted in the phase space are two sample trajectories after a kick (a) $T = 20$ minutes. The limit cycle is stable. (b) $T = 200$ minutes. We see chaotic behavior. Here, $t_d = 12$ min and $A = 10$ mg/dL. Other parameter values are as in [7].*

Main Result: Periodically kicking the stable limit cycle observed in glucose-insulin dynamics results in chaotic behavior when the kicks are sufficiently far apart temporally (representing meal ingestion). The amplitudes of the kicks similarly induce chaos in glucose-insulin limit cycles. Glucose levels more reliably oscillate when inter-meal times are relatively short and carbohydrate amounts per meal are small. This could have important clinical implications in terms of treatment of diabetic patients in the ICU.

Future Work

Physiological systems are inherently noisy. Our analysis up until now has consisted of periodic perturbations of a limit cycle. Even in such a case chaotic behavior has emerged. However, next we seek to include noise in the system in a variety of cases. For example, we will let inter-meal times be Poisson distributed, and the nutritional driver of the system will be taken to be Gaussian-distributed around a given value. We seek to learn how including noise alters glucose-insulin limit cycle behavior.

Oscillations are ubiquitous in physiological systems. We hope to implement a framework studying shear-induced uncertainty in a variety of physiologic oscillations.

Doctoral (Previous) Work

- **Axonal Length Sensing**. We provided a theoretical framework for a hypothesized mechanism for axonal length sensing proposed in [8]. The hypothesis is that axonal length information is encoded into the frequency of a chemical oscillation in the axon–as axonal length increases chemical oscillation frequency decreases. We model this as an excitatory-inhibitory chemical network where the excitation and inhibition between the chemical species are coupled to chemical transport with molecular motors. This manifests as a system of delay differential equations or, more specifically, a system of advection-diffusion equations [9]. We show the dependence of chemical oscillation frequency upon axonal length and provide a theoretical framework for how information encoded in the frequency of an oscillation can be extracted by the cell, ***i.e.*** by using the chemical oscillation as a driver for a gene network [10].

- **Synaptic Democracy**. In a series of papers [13, 14, 15, 16], we investigated the impact of allowing for reversible delivery of vesicles to target sites on the equilibrium distribution of vesicles along a cell's body. The idea was introduced in a seminal paper [13] studying the impact of allowing for reversible delivery of vesicles to ***en passant*** synapses of an axon–hence the verbiage ***synaptic democracy***. Irreversible delivery of vesicles, characterized by a simple advection-diffusion-degradation PDE, reaches an exponentially decaying equilibrium profile for vesicles. This is inconsistent with experimental findings in the peripheral sensory neurons of ***Drosophila*** [11, 12], where vesicle distribution is approximately uniform. In the model, allowing for vesicle delivery to be reversible reproduces this result, providing a mechanistic description of how such uniformity may be attained. This phenomena persists in more complicated domains such as Cayley trees and higher dimensions [15]. It also persists when synapses are gated [16] and when inter-motor interactions are considered [14].

- **Flagellar Length Control**. We developed a sophisticated model of flagellar length control that captures qualitative features of the experimental time series data on the import of intraflagellar transport (IFT) trains into flagella such as non-exponential inter-event interval statistics and time-dependent Fano factors. In particular, we modeled influx of IFT using a Cox process. Injection times of IFT into flagella were taken to be Poisson distributed with a rate determined by the concentration of particles at a structure known as the basal body where the IFTs are constructed. The latter evolves according to a stochastic birth-death process; hence, the Poisson rate itself is a stochastic process. The length of the flagellum modulates the binding rate of cytoplasmic molecules that construct IFTs to the basal body. We therefore developed a mathematical link between the length-dependent regulation of IFT transport and counting processes. We also predicted that reducing the number of binding sites on the basal body, by for example pharmacologically introducing an agonist, significantly affects length regulation of basal body binding [17].

Teaching and Outreach

A large part of being a researcher is to ensure that the generations after us maintain interest in buzzing scientific fields and propel research forward rather than stalling it. To that end, I make every effort to introduce my undergraduate students to the types of mathematical research occurring via the assignment of projects. For example, a large part of the Partial Differential Equations course I taught was the completion of a project. The project completed by the student was chosen from a laundry list of topics chosen by me. In addition to common fields such as fluids and electric potentials, the projects also covered areas of biology such as pattern formation, molecular motor transport, and chemical reaction theory. In this manner they are introduced to the ways in which math can be used to provide insights into concrete, scientific problems.

I am also a firm believer that students shy away from mathematical sciences due to not being exposed to the applicability of mathematical sciences at a young age. I have participated in Science Day at the University of Utah where I was given the opportunity to speak to middle schoolers and high schoolers about the power of mathematical modeling and how it could be used to help solve some of the big problems in the scientific community.

References

[1] R. N. Alnahhas, J. J. Winkle, A. J. Hirning, **B. R. Karamched**, W. Ott, K. Josiè, and M. R. Bennett. Spatiotemporal Dynamics of Synthetic Microbial Consortia in Microfluidic Devices. *ACS Synthetic Biology*. 8: 2051-2058. (2019)

[2] **Karamched, B. R.**, Ott, W., Timofeyev, I., Alnahhas, R. N., Bennett, M. R., and Josić, K. Moran Model of Spatial Alignment in Microbial Colonies. *Physica D: Nonlinear Phenomena*. 395: 1-6 (2018).

[3] **Karamched, B. R.**, Stolarczyk, S., Kilpatrick, Z. P., and Josić, K. Optimal Evidence Accumulation on Social Networks. *arXiv*: 1810.05909 (2018)

[4] Volfson, D., Cookson, S., Hasty, J, and Tsimring, L. S. Biomechanical ordering of dense cell populations. *PNAS* 105 (40) 15346-15351 (2008).

[5] Bogacz, R., Brown, E., Moehlis, J., Holmes, P., and Cohen, J. D. The physics of optimal decision making: a formal analysis os models of performance in two-alternative forced-choice tasks. *Psychological review*. 113 (4) 700 (2006)

[6] Lin, K. K. and Young, L. S. Shear-induced chaos. *Nonlinearity*. 21(5), 899 (2008)

[7] Keener, J. P. and Sneyd, J. *Mathematical Physiology*. Springer. (1998)

[8] Rishal,I.,N.Kam,.,M.Fainzilber.2012.Amotor-drivenmechanism for cell-length sensing. Cell Reports. 1:608-616

[9] **Karamched B R** and Bressloff P C 2015 A delayed feedback model of axonal length sensing *Biophys. J.* **108** 2408-2419

[10] P. C. Bressloff and **B. R. Karamched**. A Frequency-Dependent Decoding Mechanism for Axonal Length Sensing.. Front. Cell. Neurosci. 9:281.(2015)

[11] Maeder C I, San-Miguel A, Wu E Y, Lu H and Shen K 2014 In vivo neuron-wide analysis of synaptic vesicle precursor trafficking *Traffic* **15** 273-291

[12] Wong M Y, Zhou C, Shakiryanova D, Lloyd T E, Deitcher D L and Levitan E S 2012 Neuropeptide delivery to synapses by long-range vesicle circulation and sporadic capture *Cell* **148** 1029-1038

[13] Bressloff P C and Levien E 2015 Synaptic democracy and active intracellular transport in axons *Phys. Rev. Lett.* **114** 168101.

[14] P. C. Bressloff and **B. R. Karamched**. Model of reversible vesicular transport with exclusion J. Phys. A 49 345602 (2016)

[15] **B. R. Karamched** and P. C. Bressloff. Effects of Cell Geometry on Reversible Vesicular Transport. J. Phys. A 50 055601 (2017)

[16] P. C. Bressloff, **B. R. Karamched**, S. D. Lawley, and E. Levien. Diffusive Transport in the Presence of Stochastically Gated Absorption. Phys. Rev. E. 96 (2) (2017)

[17] P. C. Bressloff and **B. R. Karamched**. Doubly Stochastic Poisson Model of Flagellar Length Control. SIAM J. Appl. Math. 78 (2), 719-741 (2018)